A Sensorless Control Method for IPMSM with an Open-Loop Predictor for Online Parameter Identification

Aravinda Perera, Roy Nilsen

Department of Electric Power Engineering, Norwegian University of Science and Technology, Trondheim, Norway

Abstract-- **In this paper, a method is proposed to improve the performance of a mechanical transducer-less control of an interior permanent magnet synchronous machine (IPMSM) with use of a dedicated online parameter estimator (OPE). The active flux observer is employed for position estimation, along with the proposed OPE which displays high sensitivity to parameter-discrepancies, that its parameter adaptation algorithm (PAA) takes advantage of. The temperature-sensitive parameters are adapted in different speed ranges by scheduling the adaptation-gains for optimal performance. The simulation results show that the proposed method improves the torque and speed control of the drive across the torque-speed plane particularly in the presence of varying parameters.**

Index Terms— **Adaptive control, prediction error, sensor-less, soft sensor, variable speed drive**

I. INTRODUCTION

More and more mission-critical applications as such as aerospace, ship propulsion and seabed mining are opting IPMSM, due to its high efficiency and torque density. The dependability of the motor drive system has been a matter of concern in such applications, to ensure the high-performance and productivity.

Rotor-position sensor-less control methods for IPMSM become prominent in enhancing the overall reliability of the electric drive. The state-of-the-art for sensorless control is a hybrid solution which applies high frequency signal injection (HFSI) -dominant estimation at zero and low speeds and fundamental excitation (FE) -dominant estimation in remaining speeds to extract the best use of each method. Depending on the frequency of the injected signal, HFSI methods, however, can degrade the motor performance, hence it is beneficial to extend the application of FE based approach as close as possible to zero speed. The challenge is then the performance of the observer becomes increasingly sensitive to certain motor parameters.

Among the motor parameters, stator-winding resistance (R_s), permanent magnet flux linkage (Ψ_m) and quadrature-axis inductance (L_q) influence the most on sensorless control. Magnetic saturation is what can impair L_q, which implies its load dependency. Therefore, it is fair to identify L_q on the premise of a stator current or flux based mathematical function [1] based on a simpler offline experiment. Contrastingly, R_s and Ψ_m are temperature dependent. Despite the temperature variations are rather slow due to the thermal capacity, they can be unforeseen in certain ambiences as such as deep-sea. This necessitates a scheme for online R_s and Ψ_m estimation to ensure high performance sensorless control. Numerous position-observer structures inherently minimize parameter-sensitivities to attain reasonable position estimation in the low speed region. In [2], [3] the voltage model ($\mathscr{M}_u$) augmented with a drift compensation scheme is employed whereas in [4], [5], the model reference adaptive system (MRAS) is applied, and extended EMF is introduced in [6] for position estimation. Online parametric adaptation, on the other hand, is proven to enhance position estimation particularly at low speeds [7] when coupled with above position-observation schemes. MRAS methods can be extended as in [1], [8] for R_s and Ψ_m adaptation. Kalman Filter [9], [10] and recursive least square (RLS) [11], [12] based methods are alternative approaches. In [13], RLS method combined with HFSI method is employed.

In this paper, the active-flux observer in [5] is attempted to be augmented by a devoted online parameter estimator (OPE) presented in [14] for recursive identification of Ψ_m and R_s. The OPE's high sensitivity to parametric discrepancies is exploited in the chosen parameter adaptation algorithm (PAA) that adopts recursive prediction error method [15], [16]. Simulation results show that the proposed method improves the torque and speed control and the stability of the IPMSM-drive across the torque-speed plane.

II. SENSORLESS DRIVE SYSTEM

A. IPMSM Mathematical Model

The voltage model, $\mathscr{M}_u$ and current model, $\mathscr{M}_i$ of the electrical machine is in stator co-ordinates, when given in the per-unit (pu) system:

$$\underline{u}_s^s = r_s \cdot \underline{i}_s^s + \frac{1}{\omega_n}\frac{d\underline{\psi}_s^s}{dt}; \qquad \underline{\psi}_s^s = \mathbf{x}_s^s(\vartheta) \cdot \underline{i}_s^s + \underline{\psi}_m^s \qquad (1)$$

Here, ω_n is the nominal rotational frequency. The superscript and subscript denote the reference frame and the location of the quantity (*s*-stator, *r*-rotor, *m*-magnet) respectively. When the currents are chosen as the state variables, (1) becomes as follows in the rotor coordinates:

$$\underline{u}_s^r = r_s \cdot \underline{i}_s^r + \frac{\mathbf{x}_s^r}{\omega_n} \cdot \frac{d\underline{i}_s^r}{dt} + \mathbf{j} \cdot n \cdot \mathbf{x}_s^r \cdot \underline{i}_s^r + \mathbf{j} \cdot n \cdot \underline{\psi}_m^r \qquad (2)$$

Here ϑ is the electrical angle of the mechanical position $p*\vartheta_{mech}$, where p is the number of pole pairs. Electrical speed is denoted by n. The rotor-oriented inductance matrix becomes:

$$\mathbf{x}_s^r = \begin{bmatrix} x_d & 0 \\ 0 & x_q \end{bmatrix}, \ \mathbf{j} = \begin{bmatrix} 0 & -1 \\ 1 & 0 \end{bmatrix}, \ \underline{i}_s^r = [i_d \quad i_q]^T, \ \underline{\psi}_m^r = [\psi_m \quad 0]^T \quad (3)$$

B. Position Estimation Model

The position estimation adopts the MRAS based observer [5] in which a mathematical manipulation introduced in [17] is applied to remove the inherent inductance-saliency in the IPMSM model in order to simplify the arithmetic. Accordingly, a quantity called 'active flux' is defined as follows;

$$\underline{\hat{\psi}}_T^s = \omega_n \cdot \int (\underline{u}_s^s - \hat{r}_s \underline{i}_s^s + \underline{u}_{comp}^s) \cdot dt - \hat{x}_q \cdot \underline{i}_s^s = \underline{\hat{\psi}}_{s,u}^s - \hat{x}_q \cdot \underline{i}_s^s \qquad (4)$$

Here, ψ_T is the active flux component, which is nothing but the torque-producing flux component. In this active flux observer structure shown in the Fig. 1, the $\mathcal{M}_i$ and $\mathcal{M}_u$ model are employed as the reference and adaptive models respectively. Thus, the reference model is given as follows:

$$\underline{\hat{\psi}}_{s,i}^r = \mathbf{x}_s^r \cdot \underline{i}_s^r + \widehat{\underline{\psi}}_m^r \qquad (5)$$

The adaptive model is given as follows:

$$\underline{\hat{\psi}}_{s,u}^s = \omega_n \cdot \int (\underline{u}_s^s - \hat{r}_s \cdot \underline{i}_s^s + \underline{u}_{comp}^s) \cdot dt \qquad (6)$$

From which, the error, $\varepsilon_{s,o}$ is calculated and attempted to eliminate with the aid of a proportional-integral (PI) compensator.

$$\underline{\varepsilon}_{s,o} = \underline{\hat{\psi}}_{s,i}^s - \underline{\hat{\psi}}_{s,u}^s \qquad (7)$$

The $\underline{\varepsilon}_{s,o}$ is influenced by the integrator offset, parametric discrepancies, measurement errors, the dead-times in the PWM-inverter device switching and other nonlinearities in the system which are required to be compensated, at least for low speeds [17]. This MRAS-observer resembles the classical voltage-current model ($\mathcal{M}_{ui}$) in which it is typical to apply the $\mathcal{M}_i$ and $\mathcal{M}_u$ as the reference and adaptive models respectively to extract the prominent benefits in each model in exclusive speed regions. $\mathcal{M}_u$ becomes more and more R_s-sensitive when speed is lowered down to zero, opposing to the $\mathcal{M}_i$ which shows a stable parameter-sensitivity in the lower speed regions [18]. It is shown in [19] how a carefully
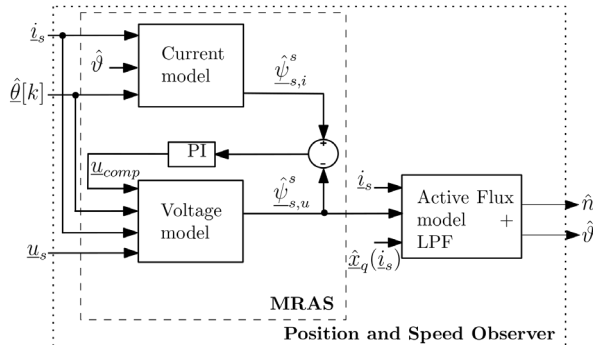
chosen P-compensator (PI in our case) can improve the flux vector estimate. Accordingly, at lower speeds, the voltage-model flux vector follows the estimation from current model and at higher speeds, that of the (drift compensated) voltage-model itself. It is essential to correct the flux estimate from the $\mathcal{M}_u$ in the best possible way as, it is seen from (4), this is the very quantity that is manipulated to obtain the active-flux, from which we yield the position and speed estimations as given in (8). The ripple in speed estimation is subsequently treated with a low-pass filter (LPF) before feeding to the OPE and the control system.

$$\hat{\vartheta} = \mathrm{atan}2\left(\frac{\hat{\psi}_{T,\beta}^s[k]}{\hat{\psi}_{T,\alpha}^s[k]} \right)$$
$$\hat{n} = \frac{\hat{\psi}_{T,\alpha}^s[k-1] \cdot \hat{\psi}_{T,\beta}^s[k] - \hat{\psi}_{T,\beta}^s[k-1] \cdot \hat{\psi}_{T,\alpha}^s[k]}{T_{samp} \cdot \left(\left(\hat{\psi}_{T,\alpha}^s[k] \right)^2 + \left(\hat{\psi}_{T,\beta}^s[k] \right)^2 \right)} \qquad (8)$$

Here, T_{samp} is the sampling time of the digital control system and $k\,T_{samp}$ is discrete-time in which k is the sample number. The value $k-1$ denote one sample time delayed quantities [5]. As you may have noticed from (5) and (6), the $\mathcal{M}_u$ is in the stator-coordinates, but the $\mathcal{M}_i$ is in the rotor-coordinates. To perform the recursive adaptation in the $\mathcal{M}_u$, the quantities in the $\mathcal{M}_i$ should be transformed from stator coordinates to rotor-coordinates and then back to the stator coordinates. The estimated position is fed back to the reference model for this reason.

C. Parameter Adaptation Model

In the proposed sensorless control method, the observer is augmented by a dedicated online parameter estimator (OPE) as illustrated in the Fig. 2. Despite the active flux observer offers satisfactory position estimation in a wide speed range [5], [17], when the Ψ_m and R_s are varying, the observer alone struggles to compensate for the discrepancies. The dedicated OPE is introduced with the motivation of relieving the observer from its parameter-correction tasks and possibly, to improve the position estimation and sensorless control in general.

The OPE proposed in [14] is used in here which contains an open-loop predictor that predicts the stator current using the full-order model, $\mathcal{M}_{u\vartheta}$ given in (9). The predicted quantities are then compared with the measured

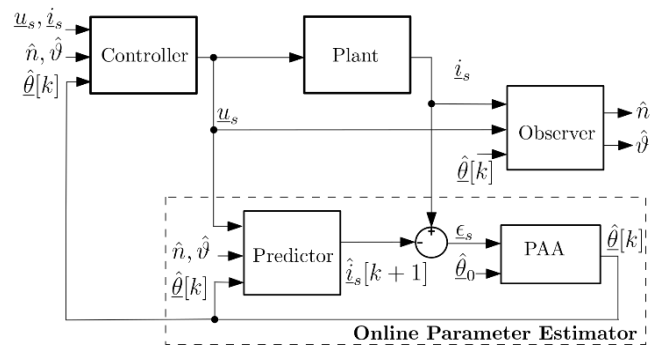Fig. 1. Observer detailed block diagram

Fig. 2. Position observer complimented with an online parameter estimation block diagram

quantities in order to generate the prediction error, $\underline{\varepsilon}_s$. Unlike in an observer, this error is not fed back to the predictor for immediate error-correction, thus $\underline{\varepsilon}_s$ becomes more sensitive to the potential parametric discrepancies in the predictor with reference to the respective physical quantities. This sensitivity is exploited by the parameter adaptation algorithm (PAA).

$$\underline{u}_s^r = \hat{r}_s \cdot \underline{\hat{i}}_s^r + \frac{\mathbf{x}_s^r}{\omega_n} \cdot \frac{d\underline{\hat{i}}_s^r}{dt} + \mathbf{j} \cdot n \cdot \hat{\mathbf{x}}_s^r \cdot \underline{\hat{i}}_s^r + \mathbf{j} \cdot n \cdot \underline{\hat{\psi}}_m^r \quad (9)$$

$$\hat{\underline{\theta}} = \begin{bmatrix} \hat{\psi}_m & \hat{r}_s \end{bmatrix}^T$$

The estimated parameters matrix, $\hat{\underline{\theta}}$, consists only the parameters that are adapted recursively in this scope.

D. Parameter Adaptation Algorithm (PAA)

The PAA in the method proposed in [14] is premised on the recursive prediction error method. The PAA in discrete form based on the Forward Euler Method, becomes:

$$\hat{\underline{\theta}}[k] = \left[\hat{\underline{\theta}}[k-1] + \mathbf{L} \cdot \underline{\varepsilon}_s^r[k] \right]_{D_M}$$

$$D_M = \left\{ \begin{array}{c} \psi_{m,\min} \le \hat{\psi}_m \le \psi_{m,\max} \\ r_{s,\min} \le \hat{r}_s \le r_{s,\max} \end{array} \right\} \quad (10)$$

Here D_M is the defined parameter space. The analytical expressions for the $\underline{\varepsilon}_s$ in steady state become:

$$\varepsilon_d = -\frac{n^2 \cdot \hat{x}_q}{\hat{r}_s^2 + n^2 \cdot \hat{x}_q \cdot \hat{x}_d} \cdot (\psi_m - \hat{\psi}_m)$$
$$- \left[\frac{\hat{r}_s}{\hat{r}_s^2 + n^2 \cdot \hat{x}_q \cdot \hat{x}_d} \cdot i_d + \frac{n \cdot \hat{x}_q}{\hat{r}_s^2 + n^2 \cdot \hat{x}_q \cdot \hat{x}_d} \cdot i_q \right] \cdot (r_s - \hat{r}_s) \quad (11)$$

$$\varepsilon_q = -\frac{n \cdot \hat{r}_s}{\hat{r}_s^2 + n^2 \cdot \hat{x}_q \cdot \hat{x}_d} \cdot (\psi_m - \hat{\psi}_m)$$
$$- \left[\frac{\hat{r}_s}{\hat{r}_s^2 + n^2 \cdot \hat{x}_q \cdot \hat{x}_d} \cdot i_q - \frac{n \cdot \hat{x}_d}{\hat{r}_s^2 + n^2 \cdot \hat{x}_q \cdot \hat{x}_d} \cdot i_d \right] \cdot (r_s - \hat{r}_s)$$

Eq (11) indicates that $\underline{\varepsilon}_s$ is influenced by ψ_m-estimate error which is coupled with the rotor speed while the r_s-estimate error is coupled with both speed and current. To rapidly identify the gain matrix $\mathbf{L}$ for accurate identification of $\hat{\underline{\theta}}$ in D_M, a sub-algorithm known as stochastic gradient algorithm (SGA) is applied, which is:

$$\mathbf{L} = \gamma[k] \cdot \frac{\mathbf{\Psi}^T[k]}{r[k]}$$

$$\gamma[k] = \gamma_0 = \frac{T_{samp}}{T_0}$$

$$\mathbf{\Psi}^T = \left[\left(\frac{d\underline{\hat{i}}_s^r[k, \hat{\psi}_m]}{d\hat{\psi}_m} \right)_{steady-state} \left(\frac{d\underline{\hat{i}}_s^r[k, \hat{r}_s]}{d\hat{r}_s} \right)_{dynamic-state} \right] \quad (12)$$

$$r[k] = r[k-1] + \gamma[k] \cdot \left\{ tr\left[\mathbf{\Psi}[k] \cdot \mathbf{\Psi}^T[k] \right] - r[k-1] \right\}$$

Here, the sensitivity of the prediction error against the estimated parameter, known as prediction-error gradient, PEG denoted by $\mathbf{\Psi}^T$ is exploited. Accordingly, the elements in $\mathbf{L}$ can be identified:

$$\mathbf{L} = \begin{bmatrix} L_{11} & L_{12} \\ L_{21} & L_{22} \end{bmatrix}, \quad \begin{array}{l} L_{11}, L_{12} = \textit{adaptation gains of } \psi_m \\ L_{21}, L_{22} = \textit{adaptation gains of } r_s \end{array} \quad (13)$$

E. Gain Scheduling

In looking at the influence on the $\underline{\varepsilon}_s$ from simultaneous parametric errors, [14] explains the necessity and sufficiency to adapt r_s only in very low speeds whereas to perform ψ_m-adaptation in the rest of the speed region. Parametric influence on the position estimation also conforms to the same order. In (2), when n becomes smaller, the back EMF-term $n \cdot \psi_m$ becomes smaller, thus the prominence of $r_s \cdot i_s$-term increases, so does the influence of r_s in the stator voltage which is key in the position estimation. The opposite phenomenon occurs when n increases to make ψ_m significant. Thus, in sensorless control based on the FE-methods, it is necessary and sufficient to perform r_s and ψ_m-adaptations in exclusive zones as shown in the Fig. 3
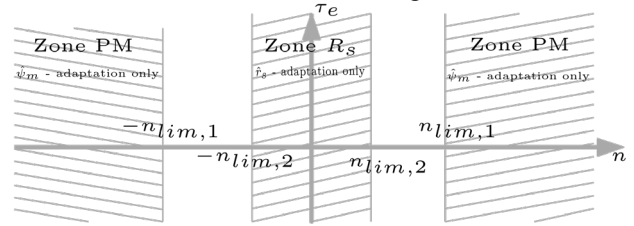

Fig. 3: Representation of zonal adaptation of R_s and Ψ_m in the speed-torque plane

Consequently, in the proposed sensorless control method, the respective adaptation gains become:

$$L_{1x} = \left\{ \begin{array}{ll} L_{1x}, & |n_{\lim,1}| > 0.1\,pu \\ 0, & otherwise \end{array} \right\}; x = 1,2$$

$$L_{2x} = \left\{ \begin{array}{ll} L_{2x}, & |n_{\lim,2}| < 0.01\,pu \\ 0, & otherwise \end{array} \right\}; x = 1,2 \quad (14)$$

It is then interesting to examine how an error in one parameter influences the other when the drive is in a speed zone where the erroneous parameter is not adapted, but the other is.

The influence from the erroneous r_s estimate on the ψ_m estimate, in Zone PM in Fig. 3, is first investigated. It is inferred in [14], that the L_{12}, which is the gain from the respective q-component has negligible influence on the ψ_m adaptation, thus only the d-component is analyzed here. Accordingly, from (11) it can be derived the unfairly adapted ψ_m at steady state due to r_s estimate-error as follows:

$$\hat{\psi}_m = \psi_m + \frac{\delta r_s}{n^2 \cdot \hat{x}_q} \cdot \left[\hat{r}_s \cdot i_d + n \cdot \hat{x}_q \cdot i_q \right], \delta r_s = r_s - \hat{r}_s \quad (15)$$

ψ_m is typically 50 to 100 times larger than r_s in per-unit. Under this circumstance, it is seen from (15) that, only when n is very small, the influence from un-adapted r_s (or non-zero δr_s) on the ψ_m-estimate becomes significant. This does not fortunately become an issue as per the zonal adaptations as in Fig. 3. Eq. (15) also indicates that the ψ_m-estimate, due to the erroneous r_s-estimate, is load dependent. Thus, for a completely fair zonal adaptation, both the speed and torque-based zones should be considered. Similarly, the influence from $\delta\psi_m$ on the r_s estimate in the Zone R_s, can be analyzed. Unlike the previous discussion, here we should consider the influence from both ε_d and ε_q [14].

$$\hat{r}_s \ = \ r_s + \frac{n^2 \cdot \hat{x}_q}{\left[\hat{r}_s \cdot i_d + n \cdot \hat{x}_q \cdot i_q\right]} \cdot \delta\psi_m, \, \delta\psi_m = \psi_m - \hat{\psi}_m$$

$$\hat{r}_s \ = \ r_s + \frac{n \cdot \hat{r}_s}{\left[n \cdot \hat{x}_q \cdot i_d - \hat{r}_s \cdot i_q\right]} \cdot \delta\psi_m \tag{16}$$

As $\delta\psi >> \delta r_s$, r_s-estimate can be unfairly impacted by the wrong ψ_m estimate across the speed regions, particularly at higher speeds. Thus, it is indispensable to cut-off the r_s-adaptation beyond a certain limit, $n_{lim,2}$, as in the Fig. 3 or else, r_s will saturate at $r_{s,max}$ (10). The penalty that the correct r_s must pay due to the wrong ψ_m estimate in the Zone R_s is however inevitable, except at standstill, under this gain-scheduling scheme.

III. SIMULATION RESULTS AND DISCUSSION

A 3-phase IPMSM drive with a 2-level inverter and quadratic or static load has been simulated in MATLAB Simulink/Simscape toolbox. Asymmetrical modulation with 3rd harmonic injection has been used. The switching frequency is 3 kHz and the sampling frequency of the digital controller is 6 kHz. The dead-time effects in the inverter have been compensated in the simulation.

Maximum-torque-per-ampere (MTPA) -control strategy is considered in this paper with the aid of the 3rd order approximation for reference current calculations given in [20]. With the simulation data in the TABLE I, the cases tabulated in the TABLE II have been simulated. The instance of the active flux observer-alone is considered as the base-case in all scenarios to comparatively investigate the performance of the proposed sensorless control method. The initial errors in the ψ_m and r_s-estimates are -10% and -20% that amount

TABLE I.　SIMULATION DATA

	Symbol	Value	Unit
Nominal voltage	U_N	690	V
Nominal current	I_N	478	A
Rated frequency	f_N	50	Hz
Pole pairs	p	1	-
Rated torque	$\tau_{e,rated}$	1818.4	Nm
Nominal speed	N	3000	rpm
Motor parameter vector	$[\psi_m \ x_d \ x_q \ r_s]^T$	$[0.66 \ 0.4 \ 1 \ 0.009]^T$	pu
Initial estimated parameter vector	$[\hat{\psi}_m \ \hat{x}_d \ \hat{x}_q \ \hat{r}_s]^T$	$[0.59 \ 0.4 \ 1 \ 0.007]^T$	pu

TABLE II.　SIMULATION CASES

	Observer Alone (Base-Case)	Observer + OPE (Proposed -Method)
Case 1 Different speed regions, initial wrong $\hat{\theta}$, Quadratic load	Case 1.1	Case 1.2
Case 2 Slow zero-crossing, dynamic θ, Constant load	Case 2.1	Case 2.2
Case 3 Very-low constant speed, dynamic θ, Constant load	Case 3.1	Case 3.2

to the initial estimations as given in the TABLE I. The PI gains of the active flux observer $k_p = k_i = 0.05$ have been identified based on simulation experiments to obtain satisfactory closed-loop performance. LPF time-constant is set to be 3.5 ms to achieve sufficiently filtered speed estimation. The zonal adaptation limits $n_{lim,1}$ and $n_{lim,2}$, are 0.1 and 0.01 pu respectively.

The state-sequence of the drive is such that, initially, the drive enters a start-up method in which the following references are fed into the vector controller: $i_q = 0$, $i_d = 0.5$, $\vartheta_{rotor} = 0$. Purpose of the start-up method is to initialize the observer and to allow r_s-adaptation at zero speed. While start-up method is enabled, after 200 ms, the speed and position estimations from the observer are released to the drive. 300 ms seconds later, the start-up method is disabled to enable the MTPA control strategy.

A. Case 1: Across different speed-regions

The rotor accelerates from 0 to 1000 rpm (> 0.3 pu) and the torque reaches 1 pu until 4 s. See Fig. 4(a). In the base-case, the wrong initial parameters continue whereas in the proposed method, they are corrected within 4 seconds from the start-up of the drive as seen in the Fig. 4(b). Due to the persistently wrong parameters, particularly due to the underestimated ψ_m, the estimated torque, $\tau_{e,est}$ (yellow curve) is continuously under the reference, $\tau_{e,ref}$ (blue), and the actual torque, $\tau_{e,act}$ (red curve) is opposingly, over the reference. This is because, the initially wrong ψ_m creates overly compensated $\tau_{e,act}$. This torque-error, $\delta\tau_e$ is conspicuous in the higher torque regions. Contrastingly, in the proposed method (Case 1.2), as soon as the estimated parameters converge with their respective physical quantities, $\tau_{e,est}$ and $\tau_{e,act}$ converge with their $\tau_{e,ref}$. The corresponding δn, $\delta\vartheta$ as in Fig. 4 (c) tell that, at higher speeds, they are not much influenced by the parameters. However, beyond 4 seconds, when the n starts decreasing, $\delta\vartheta$ gradually increases in the base-case whereas this is resiliently almost zero in the proposed method. Especially at the zero-crossing, both $\delta\vartheta$ and δn peak in the base-case, unlike in the proposed method, where the $\delta\vartheta$ is nearly indifferent. Fig. 4 (d) shows the u_{comp}, the correction term in the adaptive model, which is persistently considerable in the base-case in which the observer-alone attempts to compensate for the estimated parameter-discrepancies. u_{comp} in the proposed method, on the other hand, is nearly zero, after the initial parameter-correction, thanks to the dedicated OPE.

It is, however, interesting to note that, particularly w.r.t. ψ_m, despite the erroneous initial value is 0.594 pu (which is used in the base-case across the time span), in the proposed method, the initial estimated ψ_m is 0.474 pu which is the $\psi_{m,min}$ in (10). This overly low estimated value creates a worse-off situation at the start of adaptation, resulting in a higher torque error than that of the observer-alone method. Consequently, $\delta\vartheta$ and u_{comp} are also affected, as marked in the Fig. 4 (c) and (d).
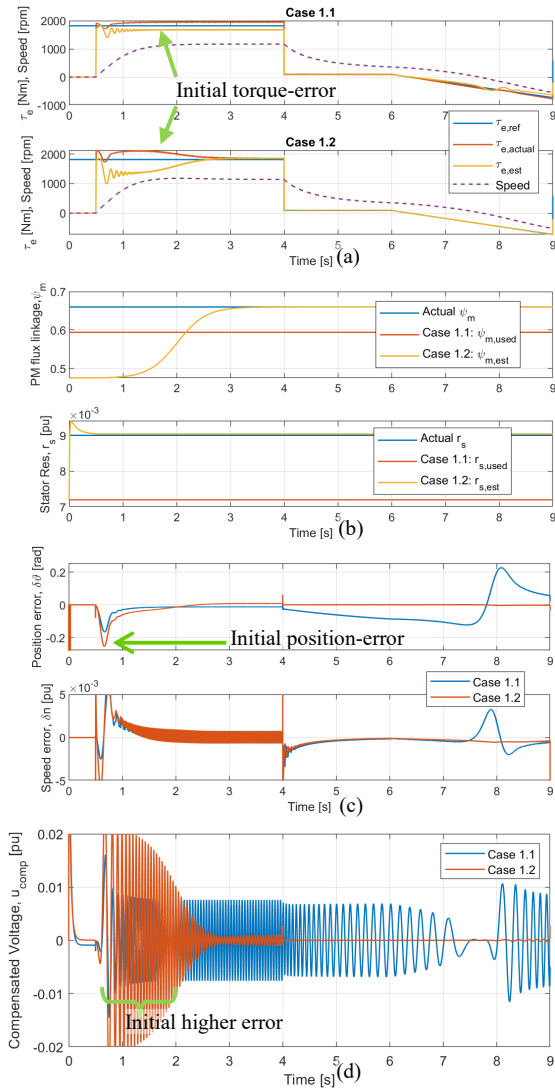
Fig. 4. Simulation results of Case 1 in time (a) Reference, actual and estimated torques and actual rotor speed (b) Actual and estimated -paramters (c) Position and speed -errors (d) Compensated voltage in the adaptive model in the observer

B. Case 2: Slow zero-crossing

Here, it takes 15 seconds for the rotor to go from +0.03 to -0.03 pu to simulate a relatively slower zero-crossing as seen in the Fig. 5(a). In addition, while the estimated parameters are aligned with them of the motor at the start of the time frame of interest, the motor parameters go through a step change: r_s increases by 5% at 5 s, ψ_m increases by 5% at 18 s. See Fig. 5(b). This scenario replicates a situation that an industrial drive can possibly undergo when the motor operates for a long time, the machine losses among other, can heat the windings and the magnets to cause parametric changes. The simulated step-change in the parameters of concern is however a hypothetical worse scenario in looking at the thermal time-constant. As a result of the zonal adaptation, there is a gap between the physical parametric change and the start of adaptation, as marked in the Fig. 5(b). In contrast, in the base-case, the model parameters do not adapt according to their respective physical parameters. Despite it is inevitable that $\delta\vartheta$ rises when crossing the zero-speed
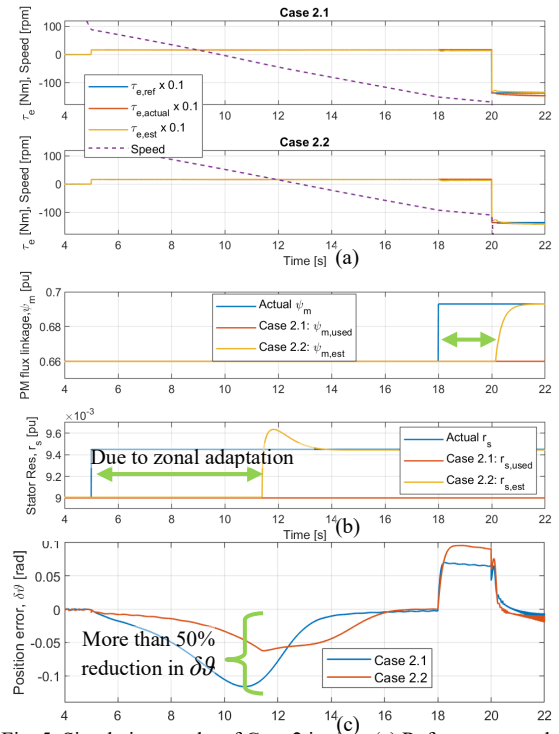

Fig. 5. Simulation results of Case 2 in time (a) Reference, actual and estimated torques and actual rotor speed (b) Actual and estimated - paramters (c) Position error

under FE-based sensorless control methods, it is evident from Fig. 5(c), with the proposed method, $\delta\vartheta$ is kept less than 50% of that in the base-case, which is a significant improvement. When the motor- ψ_m changes at 18 s, $\delta\vartheta$ is again impacted. Under the proposed method, this error is corrected as soon as the OPE enters respective adaptation zone.

C. Case 3: At Persistent Very Low Speed

A persistent, very-low speed operation under the constant load (= $0.1*\tau_{e,rated}$), a case similar to a rising electric elevator is simulated. Here, the motor r_s changes by 5% at 5 s. Fig. 6(a) brings compelling evidence to show how the proposed method succeeds in maintaining the very-low speed owing to its OPE, while the base-case fails as a result of poor τ_e control under the circumstance. Due to the absence of r_s -adaptation, it is seen in Fig. 6(c) how $\delta\vartheta$ is gradually increasing and δn is persistently erroneous in the base-case opposing to the proposed method, where these quantities are remarkably consistent and negligible. This case also illustrates the shortcoming of the zonal gain-scheduling scheme in the proposed method. Due to 5% step increase in ψ_m at 9.5 s, r_s estimate gets unfairly compensated that results in an undesired higher torque output than the reference to disturb the constant rotor speed.

IV. CONCLUSION

The active flux observer-based position estimation in combination with an open-loop online parameter estimator is proposed herein for sensorless control of IPMSM. Under dynamic operational temperature conditions, where the temperature-sensitive parameters
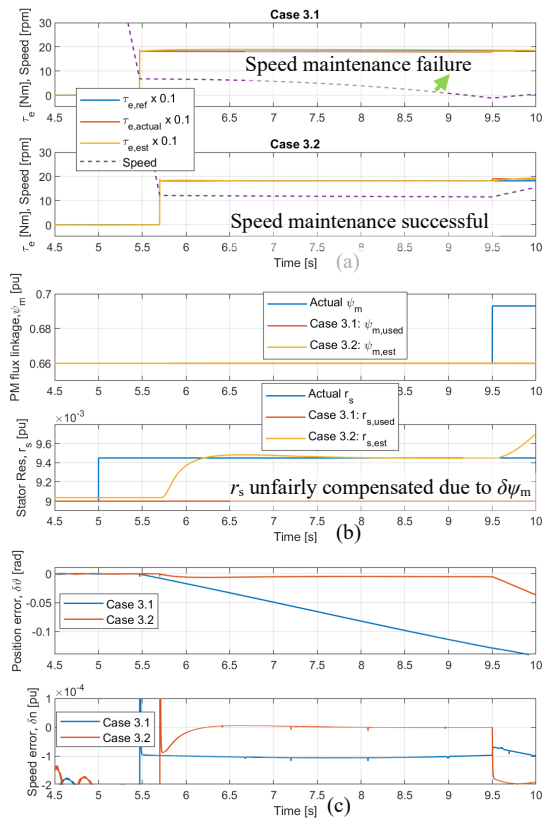
Fig. 6. Simulation results of Case 3 in time (a) Reference, actual and estimated torques and actual rotor speed (b) Actual and estimated -parameters (c) Position and speed -errors

are bound to change, the performance improvement of the drive becomes evident with the proposed method. The advantages of the online parameter estimation are seen not only in the low speed regions where r_s -compensation is required, but also in medium and high -torque and speed regions where ψ_m influence is significant. Despite the adopted zonal gain-scheduling scheme serves its purpose, an inevitable compromise in r_s-estimate is paid due to the errors in the ψ_m-estimate in the very low speed region. Methods to circumvent this undesired compensation should be further investigated.

REFERENCES

[1] A. Piippo, M. Hinkkanen, and J. Luomi, "Adaptation of motor parameters in sensorless PMSM drives," *IEEE Trans. Ind. Appl.*, vol. 45, no. 1, pp. 203–212, 2009.

[2] R. Wu and G. R. Slemon, "A Permanent Magnet Motor Drive without a Shaft Sensor," *IEEE Trans. Ind. Appl.*, vol. 27, no. 5, pp. 1005–1011, 1991.

[3] J. Hu and B. Wu, "New integration algorithms for estimating motor flux over a wide speed range," *IEEE Trans. Power Electron.*, vol. 13, no. 5, pp. 969–977, 1998.

[4] A. Piippo, M. Hinkkanen, and J. Luomi, "Analysis of an Adaptive Observer for Sensorless Control of PMSM Drives," in *31st Annual Conference of IEEE Industrial Electronics Society, 2005. IECON 2005.*, 2005, no. 4, p. 6 pp.

[5] M. C. Paicu, I. Boldea, G.-D. Andreescu, and F. Blaabjerg, "Very low speed performance of active flux based sensorless control: interior permanent magnet synchronous motor vector control versus direct torque and flux control,"

IET Electr. Power Appl., vol. 3, no. 6, p. 551, 2009.

[6] S. Morimoto, K. Kawamoto, M. Sanada, and Y. Takeda, "Sensorless control strategy for salient-pole PMSM based on extended EMF in rotating reference frame," *IEEE Trans. Ind. Appl.*, vol. 38, no. 4, pp. 1054–1061, 2002.

[7] Y. Inoue, Y. Kawaguchi, S. Morimoto, and M. Sanada, "Performance improvement of sensorless IPMSM drives in a low-speed region using online parameter identification," *IEEE Trans. Ind. Appl.*, vol. 47, no. 2, pp. 798–804, 2011.

[8] A. Khlaief, M. Boussak, and A. Châari, "A MRAS-based stator resistance and speed estimation for sensorless vector controlled IPMSM drive," *Electric Power Systems Research*, vol. 108. pp. 1–15, 2014.

[9] H. Ahn, H. Park, C. Kim, and H. Lee, "A Review of State-of-the-art Techniques for PMSM Parameter Identification," *J. Electr. Eng. Technol.*, vol. 15, no. 3, pp. 1177–1187, 2020.

[10] R. Van Der Merwe and E. A. Wan, "The square-root unscented Kalman filter for state and parameter-estimation," *ICASSP, IEEE Int. Conf. Acoust. Speech Signal Process. - Proc.*, vol. 6, pp. 3461–3464, 2001.

[11] S. J. Underwood and I. Husain, "Online parameter estimation and adaptive control of permanent-magnet synchronous machines," *IEEE Trans. Ind. Electron.*, vol. 57, no. 7, pp. 2435–2443, 2010.

[12] Y. Inoue, K. Yamada, S. Morimoto, and M. Sanada, "Effectiveness of voltage error compensation and parameter identification for model-based sensorless control of IPMSM," *IEEE Trans. Ind. Appl.*, vol. 45, no. 1, pp. 213–221, 2009.

[13] S. Ichikawa, M. Tomita, S. Doki, and S. Okuma, "Sensorless control of permanent-magnet synchronous motors using online parameter identification based on system identification theory," *IEEE Trans. Ind. Electron.*, vol. 53, no. 2, pp. 363–372, 2006.

[14] A. Perera and R. Nilsen, "A Framework and an Open-Loop Method to Identify PMSM Parameters Online," in *23rd International Conference on Electrical Machines and Systems, ICEMS, In Press*, 2020, p. 6.

[15] L. Ljung and T. Soderstrom, *Theory and Practice of Recursive Identification*, 2nd Editio. Cambridge, Massachusetts: The MIT Press, 1985.

[16] R. Nilsen and M. P. Kazmierkowski, "Reduced-order observer with parameter adaption for fast rotor flux estimation in induction machines," vol. 136, no. I, pp. 35–43, 1989.

[17] I. Boldea, M. C. Paicu, and G. D. Andreescu, "Active flux concept for motion-sensorless unified AC drives," *IEEE Trans. Power Electron.*, vol. 23, no. 5, pp. 2612–2618, 2008.

[18] T. F. Nestli and R. Nilsen, "Evaluation and comparison of predictor models for rotor flux calculation in induction motors," in *PESC Record - IEEE Annual Power Electronics Specialists Conference*, 1994, vol. 1, no. 1, pp. 729–737.

[19] F. Bauer and H. D. Heining, "Quick response space vector control for a high power three-level-inverter drive system," *Arch. für Elektrotechnik*, vol. 74, no. 1, pp. 53–59, 1990.

[20] A. Perera and R. Nilsen, "A Method Based on Prediction-Error-Gradients to Estimate PMSM Parameters Online," in *Conference Record - IAS Annual Meeting (IEEE Industry Applications Society)*, *In Press,* 2020, pp. 2–8.